Faculdade de Engenharia da Universidade do Porto

Estimation of energy production in aerial systems of Wind Energy

João Pedro Rodrigues Machado

Dissertação realizada no âmbito do
Mestrado Integrado em Engenharia Electrotécnica e de Computadores
Major: Energia

Supervisor: Cláudio Domingos Martins Monteiro
Second Supervisor: Fernando A.C.C. Fontes

Junho de 2019

Resumo

O impacto ambiental resultante da produção de energia elétrica através de combustíveis fósseis determinou uma mudança na forma de obtenção desta energia aparecendo assim as energias renováveis. O vento é a alternativa de energia renovável mais barata para a produção de energia elétrica em larga escala sendo que este é usado na energia eólica. Esta energia é principalmente extraída em terra a baixas altitudes por turbinas eólicas montadas em torres com algumas dezenas de metros (50-120 m). O vento em altas altitudes tem maior velocidade quando comparado com o vento próximo ao solo e, ainda mais importante, é mais estável e consistente.

Em busca de soluções inovadoras para geração de energia a partir de energias renováveis, nomeadamente para extrair energia eólica em grandes altitudes, estão a ser desenvolvidos diversos projetos na área de AWES (*Airborne Wind Energy Systems*). UPWIND, desenvolvido na Universidade do Porto, é um destes projetos e esta dissertação encontra-se inserida neste. Caracteriza-se por envolver um kite, similar aos usados no kitesurf, conectado a um gerador usando um cabo. Quando o kite sobe com o vento, o cabo é largado produzindo energia. O cabo é recolhido quando atinge seu comprimento máximo e, em seguida, o processo reinicia novamente.

O objetivo desta dissertação consiste em desenvolver uma metodologia de estimativa de produção do AWES já modelizado no UPWIND, especificamente um Pumping Kite Generator. É criada uma metodologia detalhada de estimativa da produção simulando o ciclo completo de largada e recolha, simulando para as diversas alturas da trajetória do AWES. Para validação, foi simulada a produção ao longo de uma série de 10 minutos ao longo de 1 ano completo. Os resultados foram comparados com uma metodologia simplificada de estimativa de produção usando uma curva de potência aplicada a uma velocidade média a uma altura média.

Os resultados obtidos tiveram como finalidade comparar os dois métodos usados para estimar a produção aplicada na simulação, assim como aplicar as velocidades de largada e recolha obtidas anteriormente, parâmetros muito importantes para a obtenção da energia produzida.

Por fim, foi possível criar uma metodologia detalhada de estimativa de potência que pode ser aplicada a casos de AWES em que a posição varia ao longo do tempo e em que é necessário estimar as novas veocidades de vento na posição em que está. Isto é algo bastante diferente dos procedimentos de estimativa de potência clássicos em que se usa uma curva de potência ajustada para uma altura do AWES fixa.

Abstract

The environmental impact resulting from the production of electricity through fossil fuels has led to a considerable change in the way energy is obtained. Nowadays, renewable energies play a major role in the production of large-scale electric power, notably wind energy due to being one of the cheapest solutions. This energy is mostly mined at low altitudes by wind turbines mounted on towers with a few tens of meters (50-120 m). The wind at high altitudes has a higher speed when compared to the wind near the ground and, more importantly, is more stable and consistent.

In search of innovative solutions for generating energy from renewable sources, namely to extract wind energy at high altitudes, several projects are being developed in the area of AWES (Airborne Wind Energy Systems). UPWIND, created at the University of Porto, is one of these projects and this dissertation is a part of it. It is characterized by involving a kite, similar to those used in kitesurf, connected to a generator by means of a cable. When the kite rises with the wind, the cable is dropped, thereby producing power. The cable is collected when it reaches its maximum length, and then the process restarts again.

The objective of this dissertation is to develop an AWES production methodology already modelled in UPWIND, specifically a Pumping Kite Generator. A detailed production estimation methodology is created by simulating the complete start and take cycle, replicating the various heights of the AWES trajectory. For validation, the production was simulated over a series of 10 minutes during a full year. The achieved results were compared with a simplified production estimation methodology applying a power curve calculated at a mean height and velocity.

The obtained results had the purpose of comparing the two methods used to estimate the production applied in the simulation. Likewise, the reel out and reel in velocities, which are very important parameters to define the energy produced, were calculated.

Finally, it was created a detailed power estimation methodology that can be applied to AWES cases, in which the position varies over time and, where it is necessary to estimate new wind speeds for each position. This is quite different from the classical power estimation procedure where a power curve is set for a fixed AWES height.

Acknowledgements

I would like to thank my thesis advisor Prof. Cláudio Monteiro for all the orientation and availability providing guidance, as well as recommendations and several revisions throughout the semester. I would also like to thank Prof. Fernando Fontes for steered me in the right direction. The support of FCT through FEDER/Compete2020 grant PTDC-EEI-AUT/31447/2017 - UPWIND in research associated to this project is also acknowledged.

I would like to thank my friends and colleagues, those who walked with me on this long and challenging journey. Thank you for showing me that friendship and companionship are something that I must preserve for life.

Finally, I give my warmest thanks to my family, in particular to my brother and parents, because without them nothing I have achieved so far would have been possible.

"I've failed over and over and over again in my life and that is why I succeed."
Michael Jeffrey Jordan

Contents

List of Figures

List of Tables

Abbreviations and Symbols

HAWT	Horizontal Axis Wind Turbine
VAWT	Vertical Axis Wind Turbine
AWES	Airborne Wind Energy Systems
GG	Ground Generation
FG	Flying generation
PKG	Pumping Kite Generator
VTOL	Vertical Take Off
T	tether tension [N]
L	lift force [N]
D	drag force [N]
ρ	air density [kg m^{-3}]
A	kite area [m^2]
P_c	mechanical power [W]
v_w	wind speed [m s^{-1}]
v_{out}	reel out speed [m s^{-1}]
v_{in}	reel in speed [m s^{-1}]
C_L	aerodynamic lift coefficient
C_D	aerodynamic drag coefficient
E_c	Energy produced over one cycle [J]
l_c	tether length [m]
t_c	duration of one cycle [s]
P_w	Power density of the wind [$kg \cdot m^{-1} s^{-3}$]
h	height above ground level [m]
p	power law exponent
β	elevation angle [°]
P_{mo}	Percentage of maximum power output [%]

Chapter 1

Introduction

The world we live in is becoming more and more dependent on electrical energy, which still heavily relies on outdated techniques involving the burning of fossil fuels. The production of these fuels has frequently resulted in a drastic rise in emissions from greenhouse gases as well as disastrous environmental impacts [1].

In order to achieve a sustainable lifestyle, several renewable sources of energy have been explored throughout the last decades. One of these has been the conversion of wind kinetic energy into electric energy using wind turbines and reaching 539 GW installed worldwide in 2017. These numbers translate in covering more than 5% of the global electricity demand [2].

The beginning of the adaptation of the wind mills for electric power generation was initiated in the late nineteenth century, in the USA [3]. After a while, the technological developments achieved in the wind turbines allowed them to distinguish in two main types: the horizontal axis wind turbine (HAWT) and the vertical axis wind turbine (VAWT) [4].

There are generally two core kinds of VAWTs, named as the Savnoius and the Darrieus and they commonly function nearer to the ground where the wind is lower. About the HAWTs, the motor wind turbines are the recent form of horizontal turbines that are used to generate electricity at commercial levels. These are mainly three-blade turbines and they make use of computer monitored motors for functioning [5].

Currently, there are many proven advantages in using HAWTs because three-bladed turbines with horizontal axis show smoother and quieter operation, with minimum aerodynamic interference. Also, the variable pitch in the blades allows to collect the maximum amount of energy from wind [4].

The wind velocity is stronger in higher altitudes which means that the energy extracted from the turbines will also be greater in increased peaks. This has caused an increase of the turbine's heights allowing larger power outputs and generally higher capacity factors.

Despite the greater outcomes in terms of electricity produced, higher towers require more materials and cause larger expenditures which may make certain projects of higher turbines unfeasible above certain boundaries.

To surpass this difficulty, different kinds of Airborne Wind Energy Systems (AWES) are being developed, permitting the exploration of higher winds with a light infrastructure. However, there is a major struggle in the development of the system´s control which leads to a great window of opportunity to improve its autonomous operation.

1.1. Motivation

This dissertation is motivated by the need to understand the viability of these systems considering the evolution of AWES. Some questions are raised to explore this possibility as if it's possible to create systems completely autonomous, what is the energy conversion efficiency, the level of maintenance that these systems require and the parameters that influence the power output. All these studies converge to know if it's feasible to create wind farms with AWES and what level of complexity adds to a singular airborne wind energy system.

1.2. Objectives

The main objective of this thesis is to answer with accuracy at some questions raised in the motivation with a greater focus on the energy problems. It will be constructed the power curve of an AWES in different conditions of wind in order to know the system´s viability and it will be applicated to calculate the total power output over a year with a provided real wind data. A statistical analysis of the data wind will also be studied to understand its importance to the power output.

1.3. Layout

The document layout follows a chapter structure and the references are presented after the last chapter. In chapter 2, a background research regarding the current situation of the airborne wind energy systems all over the world is presented. The major companies developing these systems are introduced and their devices characterized. In chapter 3, the reeling in and out speeds are calculated, as well as the power curve of the system depending on different ratios. Its operational limitations are also discussed. In chapter 4, the power curve previously created, is applied to real wind data in order to estimate the annual average power output of the system and the wind speed is analyzed. The concluding chapter is chapter 5, where considerations towards the kite´s theoretical model are offered.

1.4. UPWIND project framework

This dissertation is part of the UPWIND Project [6], which aims at exploring Airborne Wind Energy Systems. The project focuses on systems based on a tethered wing flying at a high-speed crosswind motion and its motivated by the capacity of these systems to reach heights that no other power generating device can reach.

For efficiency reasons, it is desirable that the kite follows a pre-defined path in space. Knowing the maximum power that can be extracted from the wind is obtained when the kite moves in a perpendicular direction, the optimal trajectory is periodic, and it follows a pre-defined path.

Chapter 2

Airborne Wind Energy Systems

AWES are electro-mechanical machines that transform wind kinetic energy into electrical energy and are composed by a mechanically and/or electrically connected ground station and aircraft. These systems broadly fall into two categories: static and crosswind. Electricity production for crosswind devices can happen either via ground-based generation (Ground Generation-AWES) or onboard generation (Flying Generation -AWES).

2.1. Static Airborne Wind devices

The primary benefit of these devices over the conventional wind turbines is that they have the possibility to access the higher and more persistent wind resource that exists high above even the largest conventional wind turbines. Their turbines are lifted high above the ground using lighter-than-air balloons to stay aloft and are connected to the ground electrically and mechanically using one or more tethers [7].

Altaeros is one of the main companies developing these devices having already a technology named Buoyant Airborne Turbine (BAT) as it shown on Figure 1. The Altaeros BAT can reach 600 meters high and has already an automated control system that ensures safe and efficient operation. In Figure 2 it is illustrated a comparison of this system with conventional wind turbines heights. This model is approximately 15 by 15 meters, is containerized, and does not require a crane or foundation for installation [8].

Figure 1 – Altaeros BAT device [9]

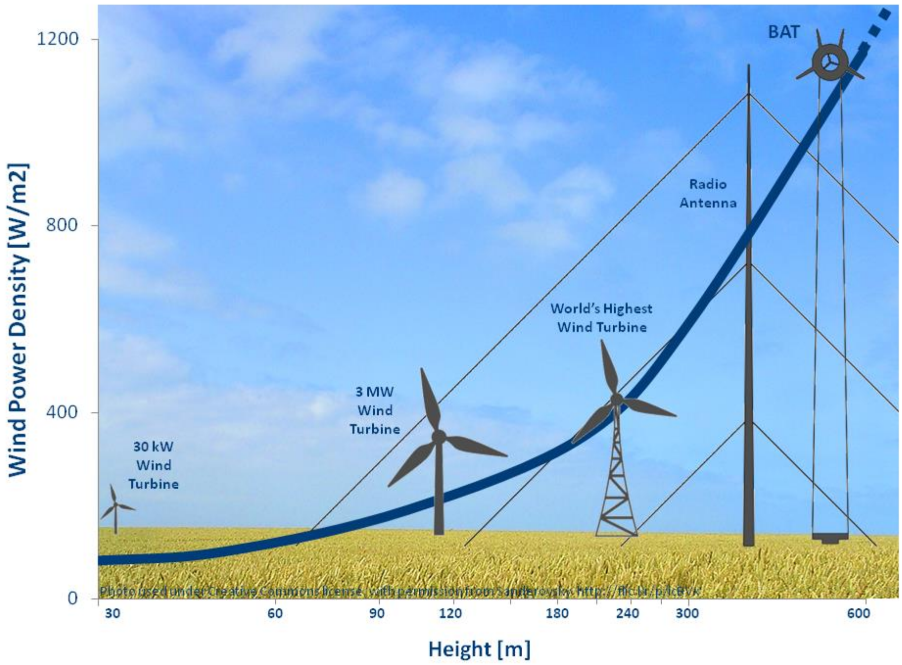

Figure 2 – Comparison of operating heights between Altaeros BAT and other conventional systems [9]

2.2. Crosswind Airborne Wind devices

These types of systems have the ability to stay in the air by flying across the wind, generating enough lift to stay high up and producing electricity. The crosswind motion allows these devices to produce between three and five times more power than the static wind devices previously indicated at the same height [7]. These devices also can sweep a greater effective area increasing the potential power output [10].

2.2.1. GG – AWES

In these ground generation systems, the electrical energy is produced exploiting aerodynamic forces that are transmitted from the aircraft to the ground through tethers. These systems are usually divided into fixed or moving-ground-station devices [11].

Fixed ground station devices or Pumping Kite Generators (PKG) are systems based on a two-phase cycle composed by a generation phase and a recovery phase. The first one is where the electrical energy is produced and the second one is distinguished by a small amount of energy that is consumed in order to retrieve the airfoil. A PKG system normally relies on a tethered airfoil whose tether is reeled around a winch drum which in turn are connected to motor-generator axes.

During the generation phase the airfoil is controlled in order to produce a lift force and subsequently a traction force on the tether that induce the rotation of the electrical generator.

To maximize the lift force, the airfoil is set into a crosswind flight following an eight-shaped path since this mode generates a stronger apparent wind [12]. This path pursues a trajectory that maximizes the time in which the kite is moving in a crosswind regime [13].

During the recovery phase, the generator begins to work as a motor rewinding the tether(s) and bringing the airfoil to his original position. It is important to control the airfoil during this phase in order to minimize the traction, thus reducing the energy required to feed the motor. This two-phased cycle can be observed in the Figure 3.

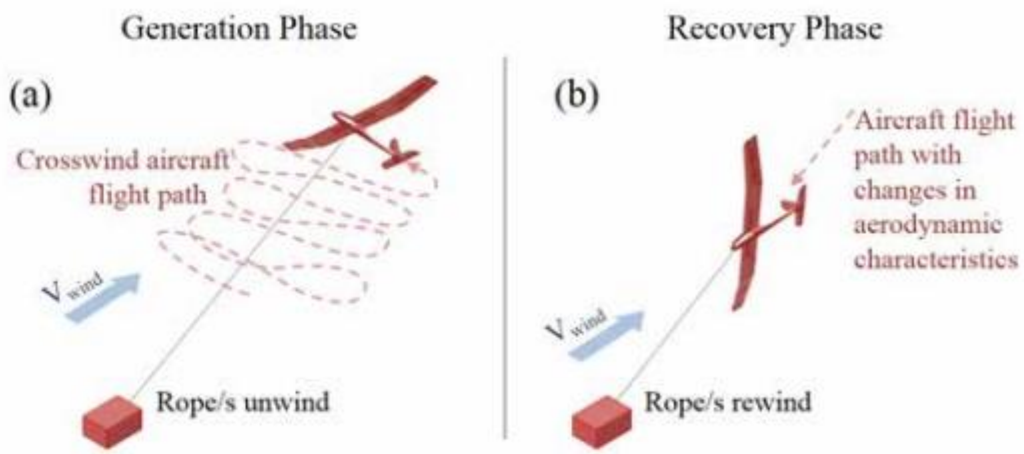

Figure 3 – Representation of a two-phased cycle airborne device [11]

Moving ground station systems have the main purpose to provide a more stable output than the PKG, simplifying the connection to the grid. In these systems, the generation of the electric power is based on the ground station movement rather than the unwinding of a rope. The ropes are eventually used only to control the aircraft trajectory.

There are two kinds of moving ground stations systems, the vertical axis generator and the rail generators. The first system is where the aircraft is connected to the periphery of a large generator with a vertical axis. The aircraft forces make the ground station rotate along with the rotor and thus inducing electrical energy. The second system, inspired on Pocock's Charvolant [14], consists on the movement of a railed vehicle integrated on an open or closed loop rail system and the electric energy is generated from vehicle motion.

2.2.2. FG – AWES

FG-AWES produce electric energy onboard of the aircraft during its flight, transmitting it to the ground through one or more electric cables. There is some variety of flying principles in these systems as wings lifted with multiples generators attached or the buoyancy of lighter-than-air structures. However, there are complications generating power on the aircrafts such as the need to transmit electrical energy to the ground without a fixed structure or the device´s mobility due to the increased weight.

2.3. AWES under development

There are an increasingly large number of research groups and companies developing AWES around the world as shown in Figure 4. This is caused by the theoretical capability of achieving the megawatt scale supported by many publications presenting analyses with MW outputs [15-17]. This characteristic is uncommon in renewable energy and provides a reason for commercial development.

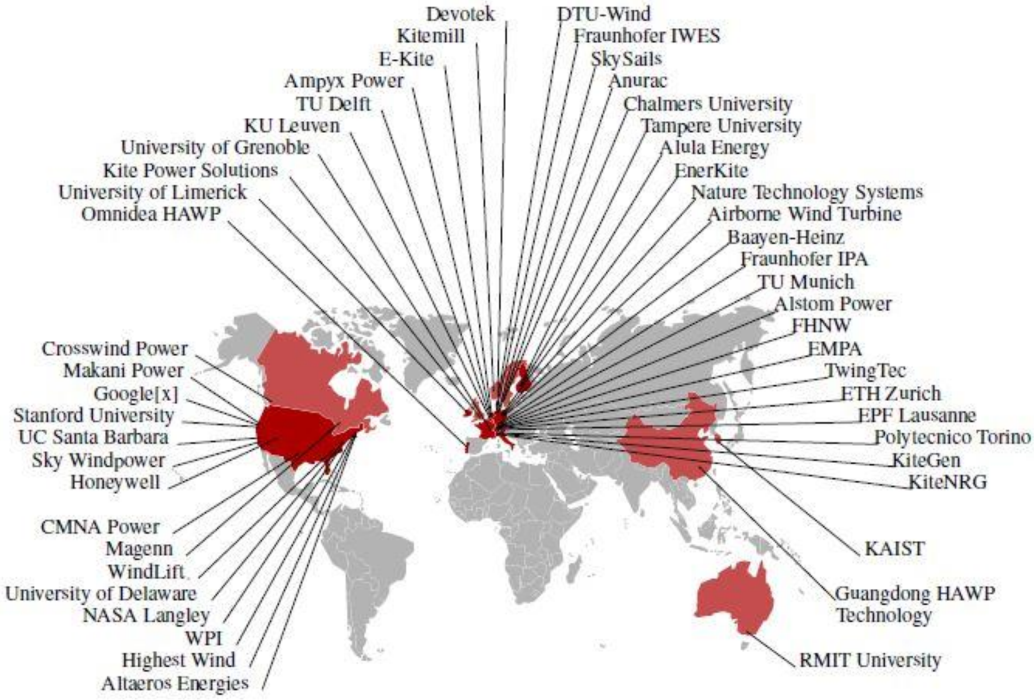

Figure 4 - Airborne wind energy research and development activities [18]

2.3.1. GG-AWES under development

Ampyx Power

This dutch company was the first one to develop a pumping glider generator, creating already three generations of prototypes (AP0-AP2). Currently, they are testing the prototype AP3, seen in Figure 5, being the objective to demonstrate the safety and autonomous operation of the system [19]. The aircraft, consisting in a wing with 12 m^2 surface area and two fuselages, is equipped with an auto-pilot in order to fly completely automatically. It moves in a regular cross wind pattern and it is tethered to a generator on the ground. It was installed a catapult for take-off and they have a propulsion system to climb up. The tether is wrapped around a drum that rotates when tension is applied by the aircraft. The motor/generator combination is responsible for the efficient conversion of tether tension into electrical power during the reel-out phase and for the efficient reel-in of the tether during the retraction phase. This process is repeated several times as the pumping cycles of a kite.

Ampyx Power intends to develop a fifth generator prototype, a 35 m^2 wingspan AP-4 PowerPlane with a ‘wind turbine equivalent’ power of 2 MW.

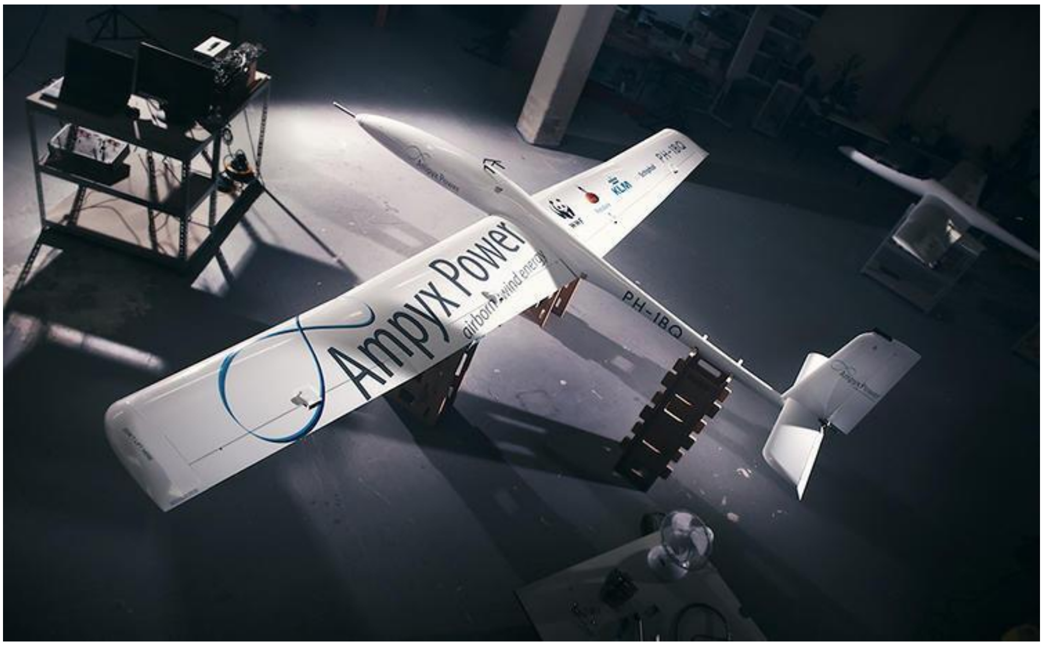

Figure 5 – Prototype AP3, Ampyx Power [19]

EnerKite

The German company EnerKite developed a portable pumping kite generator, EK30, with rated continuous power of 30 kW as seen in Figure 6[20]. This kite is also operated in two-phases. During the power phase the wing flies cross-wind, unfurling the lines with optimal force and speed. During the recovery phase the wing returns to the starting point as fast and smooth as possible with minimal energy expenditure. The ground station, which is installed on a truck through a pivotal joint, generates electrical power from the torque of the unfurling lines whilst steering the wing using differential drum drives.

EnerKite aims to scale the technology into a 500kW system [21].

Figure 6 – Ek30 model [20]

TU Delft

Delft University of Technology and Karlsruhe University of Applied Sciences have initiated a cooperative project to continue the development and testing of a mobile 20 kW experimental pumping kite generator, as shown in Figure 7. This prototype is based on a single tether and an airborne control pod, but they also control the angle of attack for powering and depowering the wing during production and recovery phase, respectively. The system operates in periodic pumping cycles alternating between reel-out and reel-in of the tether [22].

Figure 7 – TU Delft kite [23]

Kite Power Systems

This UK company founded in 2011 is also developing a pumping kite generator. It presents many similarities with other companies making PKG. Their prototype features a kite, tethers and robotic actuation for purposes of control.

Recently, this company received a £5 million investment from three energy firms, E.on, Schlumberger and Shell. The start-up’s plan is to build one of the world's first kite power stations using technology it believes could collectively generate hundreds of megawatts of energy by 2030 [24].

e-Kite

e-Kite, a company founded in 2013 in the Netherlands, is manufacturing a 100 kW GG-AWES, which can generate electricity for about a hundred households. This e100 model (Figure 8) is targeted at farmers, landowners, communities and companies in rural areas.

The company is now focusing on a 1-rope rigid wing with vertical take-off capabilities that will fly at low altitude [25].

Figure 8 – e100 model, developed by e-Kite [25]

KiteGen Research

Regarding moving ground station systems, the Italian company is studying a system based on a vertical axis concept driven by forces which come from tethered aircrafts. This concept has no prototype under development, but studies show that 100 kites with 500 m^2 area could generate 1000 MW of average power in a wind with speed of 12 m/s [26]. The following picture shows the theoretical concept of the system:

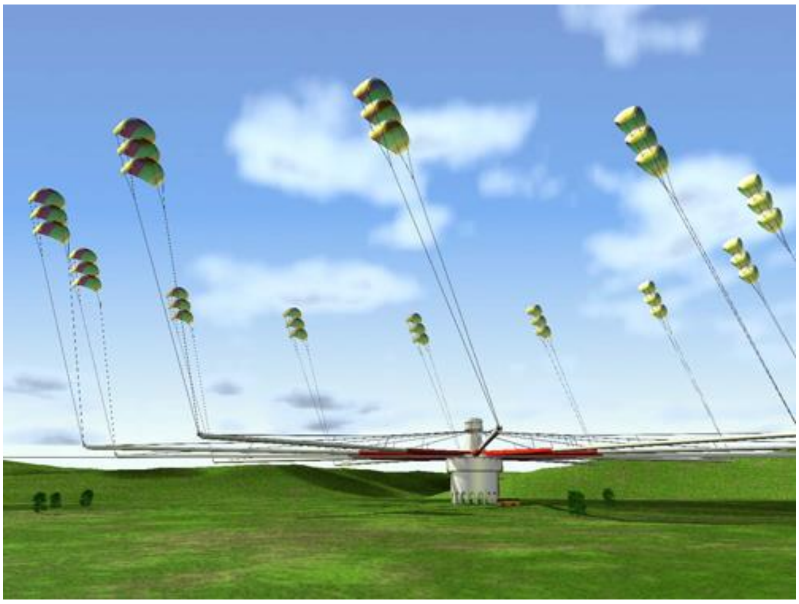
Figure 9 – Theoretical model approached by KiteGen [27]

In Figure 10 it is possible to understand the dimensions that this project can achieve compared to a single wind turbine, with an estimated area of 1 km^2 and reaching heights of 1000 meters.

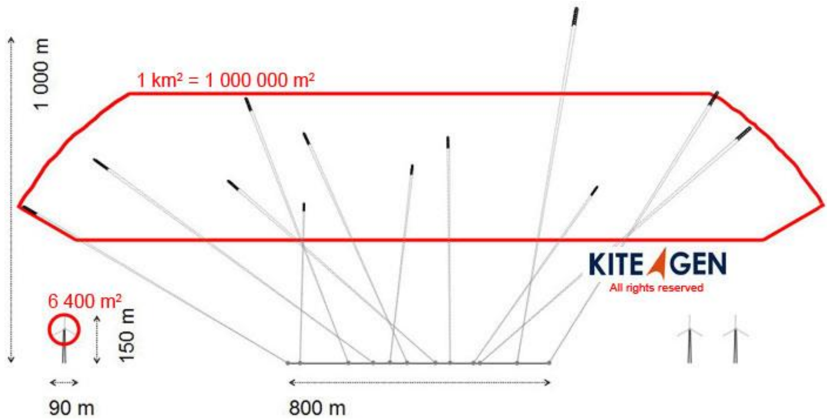

Figure 10 – Possible dimensions of the KiteGen project [28]

Besides all these companies mentioned previously, there are a few research groups worth mentioning, such as the Freiburg University and the recent group from University of Porto, UPWIND [6] in which this dissertation is related. All these research groups focus on PKG systems.

2.3.2. FG-AWES under development

This subsection provides a closer look in flying generator airborne wind systems, more specifically Makani Power, an American company which as conquered many breakthroughs in these types of systems.

Altaeros is also a company developing FG-AWES. The projects´ specifications and goals were referenced in Section 2.1.

Makani Power

The Makani AWT design consists of a rigid airframe with on-wing rotors and generators, attached to the ground by a tether. The airframe (or wing) flies circles similar to the tip of a wind turbine blade. The on-wing generators are driven by aerodynamic rotors, adding drag to the wing and generating electrical power that is transmitted down conductors on the tether [10].

In order to take off, the wing plane is in a vertical position and is driven by propellers thrust and the landing part is assured by using the plane as a quadcopter as shown in Figure 11 – Airborne device prepared for take-off [29].

Makani developed an 8 meters wingspan, 20 kW prototype named “Wing 7” that demonstrated the capability of fully automatic control and power production. After these results, Google decided to acquire Makani in 2013, translating into additional investments and projects with more ambitious goals.

One of these projects is the M600 (Figure 12 -- M600 model, developed by Makani Power [29]), a 600 kW prototype with eight turbines, each with five propeller blades, and has a wingspan of 26 m. The system has a 500 meter flexible tether to constrain the plane in flight [29].

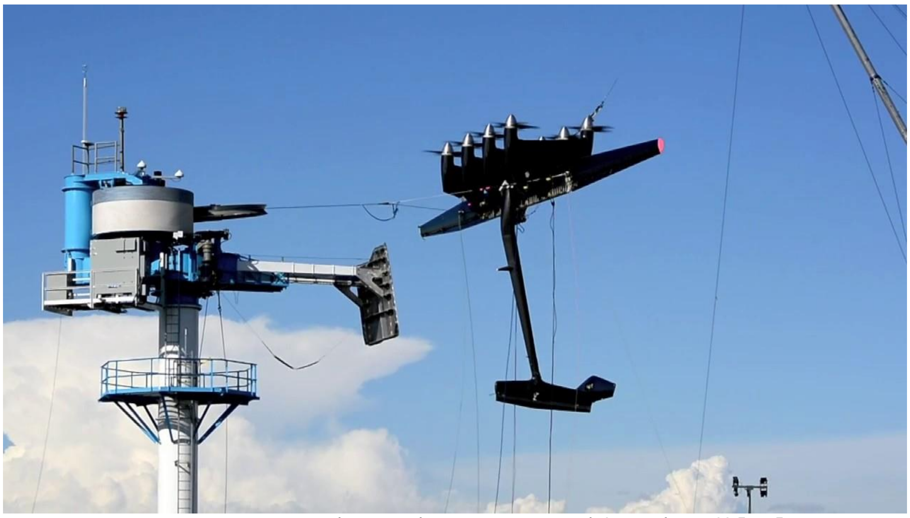

Figure 11 – Airborne device prepared for take-off [29]

Figure 12 -- M600 model, developed by Makani Power [29]

Makani Power is, without a doubt, one of the most promising companies developing AWES and has already plans to produce an offshore commercial version of AWT with a nominal power of 5 MW featuring 6 turbines and a wingspan of 65 m.

Omnidea

In Portugal, a company named Omnidea developed a lighter than air cylindrical aerostat that explores the Magnus effect. Among other applications, this inflatable called LEMAP (Long Endurance Medium Altitude Platform) can be used to generate electricity [30].

Chapter 3

Dynamic Model of the Kite Power System

As it was mentioned before, the Pumping Kite Generator under study has, in his composition, a kite and a tether connecting the kite to a stationary ground station. In addition, this station is composed by a winch drum, a generator and several electronic components necessary for the grid connection.

Firstly, in this chapter, the acting forces on the kite´s system are calculated and analyzed in Section 3.1. The reeling in and out speeds, necessary for executing the two phases over one cycle, are studied in Section 3.2 and in Section 3.3 are presented the limitations regarding the power output of the system. Section 3.4 calculates and presents the power curves of the system for different parameters. Finally, in Section 3.5, an equation to calculate different reeling in speeds above a certain nominal wind speed is derived.

3.1 Acting Forces

Following Loyd´s analytic model [12], the main forces are shown in Figure 13 - Forces and velocities acting on a flying kite [31]are the tether force *T*, the lift force *L* and the drag force *D*.

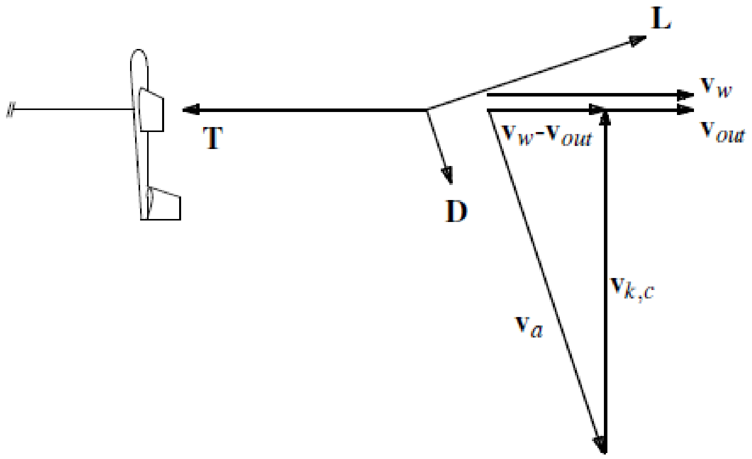

Figure 13 - Forces and velocities acting on a flying kite [31]

The wind speed is represented by v_w, the reel out speed of the tether in the traction phase of the pumping cycle is v_{out} and for large ratios of lift to drag, v_a, the apparent wind speed, is nearly equal to $v_{k,c}$. Subsequently

$$v_a \simeq v_{k,c} = (v_w - v_{out})\frac{C_L}{C_D} \tag{3.1}$$

It is possible to observe that the kite's speed is directly proportional to the lift to drag ratio of the wing, whereas the reel out speed v_{out} reduces it.

The tether force *T* is, for high lift to drag ratio, approximately equal to the lift force *L* given by

$$T \simeq L = \frac{1}{2}\rho v_a^2 A C_L \tag{3.2}$$

Where ρ is the density of the air and *A* the wing area.

The mechanical power *P* obtained in the traction phase of the pumping cycle is given by

$$P = T v_{out} \tag{3.3}$$

It is easily observed from equations 3.1 and 3.2 that the smaller reel out speed, the larger the tether force *T*. From equation 3.3 it is possible to conclude that a reel out speed equal to zero, results in no generation of mechanical power. Thus, an optimal reel out speed $v_{out,opt}$ was calculated through equation 3.4, according to Loyd´s analysis, in order to produce the maximum mechanical power.

$$v_{out,opt} = \frac{1}{3}v_w \tag{3.4}$$

Hence, the equation to calculate the maximal mechanical power is presented below:

$$P = \frac{1}{2}\rho v_w^3 A \frac{4}{27}\frac{C_L^3}{C_D^2} \tag{3.5}$$

All the equations mentioned above allow concluding that the pattern of a kite flying crosswind and the C_L/C_D are extremely important in order to produce power. Nevertheless, Loyd´s studies only approached the reel out phase not describing the retraction one.

In the following analyses, according to [31], the pumping cycle is optimized taking into account not only the traction phase but also the retraction phase too. There are some simplifications that remain from Loyd´s study. The drag of the tether is ignored, the gravitational forces are neglected, and C_L and C_D are kept constant during the traction and the retraction phase.

3.2. Reeling in and out speeds

The traction (reel out) and the retraction (reel in) phases are considered to complete a full cycle [31]. The objective of this section is to calculate the reel out and in speed, v_{out} and v_{in} respectively, where the average mechanical power over one cycle is maximal. This mechanical power will be named as P_c and two dimensionless factors will be considered: γ_{out} and γ_{in}.

$$\gamma_{out} = \frac{v_{out}}{v_w} \tag{3.6}$$

$$\gamma_{in} = \frac{v_{in}}{v_w} \tag{3.7}$$

Regarding the traction phase, the tether force is derived from equation 3.1 and 3.2:

$$T_{out} = \frac{1}{2}\rho v_w^2 A (1-\gamma_{out})^2 F_{out} \tag{3.8}$$

With the dimensionless force factor F_{out}

$$F_{out} = \frac{C_L^3}{C_D^2} \tag{3.9}$$

The tether force follows a similar derivation regarding the retraction phase:

$$T_{in} = \frac{1}{2}\rho v_w^2 A(1+\gamma_{out})^2 F_{in} \tag{3.10}$$

Being the dimensionless force factor F_{in} given by

$$F_{in} = C_D \tag{3.11}$$

The previous equation is an ideal assumption that the drag of the kite is the only force that needs to be challenged in order to reel in. However, F_{in} represents the minimal tether force required to reel in the kite in a way that does not compromise the all system.

These dimensionless force factors can be determined with physical experimentations by measuring the tether force at a given wind speed while the kite is flying crosswind. On the other hand, the lift and drag coefficients in the flying kite are sensitive to the directions of the apparent wind making it difficult to calculate.

For the reason mentioned above, theoretical values between 0 and 100 of the F_{out}/F_{in} ratios will be put into test to understand the influence in the system´s efficiency in the pumping cycle.

Considering l_c as the tether length during the cycle, the energy produced over one power cycle can be determined by the following expression:

$$E_c = (T_{out} - T_{in})l_c = \frac{1}{2}\rho v_w^2 A((1-\gamma_{out})^2 F_{out} - (1+\gamma_{in})^2 F_{in})l_c \tag{3.12}$$

The duration of the cycle, represented by t_c, is calculated by:

$$t_c = \frac{l_c}{v_{out}} + \frac{l_c}{v_{in}} = \frac{l_c}{v_w}\left(\frac{\gamma_{out}+\gamma_{in}}{\gamma_{out}\gamma_{in}}\right) \tag{3.13}$$

Knowing that the average power $P_c = \frac{E_c}{t_c}$ and assuming the new variable $P_w = \frac{1}{2}\rho v_w^3$ as the power density of the wind, one can be calculated by the expression:

$$P_c = P_w A(F_{out}(1-\gamma_{out})^2 - F_{in}(1+\gamma_{in})^2)\left(\frac{\gamma_{out}\gamma_{in}}{\gamma_{out}+\gamma_{in}}\right) \tag{3.14}$$

Normalizing P_c:

$$\frac{P_c}{P_w A F_{out}} = f_c = \left((1-\gamma_{out})^2 - \frac{F_{in}}{F_{out}}(1+\gamma_{in})^2\right)\left(\frac{\gamma_{out}\gamma_{in}}{\gamma_{out}+\gamma_{in}}\right) \tag{3.15}$$

Where the new variable f_c represents the power factor.

Considering that there is no resistance in the reeling in phase and consequently an infinite speed pulling back the tether ($F_{in} = 0$, $\gamma_{in} \to \infty$), the dimensionless factor γ_{out} for maximal power assumes the value of 1/3 (equation 3.4).

Thus, according to equation 3.5:

$$f_c^{max} = \max_{\gamma_{out}} \left\{ \frac{P_c}{P_w A F_{out}} \right\} = \frac{4}{27} \tag{3.16}$$

To calculate the maximal cycle power for force factors $F_{out}, F_{in} > 0$, the following equation must be followed:

$$f_c^{max} = \max_{\gamma_{out}, \gamma_{in}} \left\{ \left((1-\gamma_{out})^2 - \frac{F_{in}}{F_{out}} (1+\gamma_{in})^2 \right) \left(\frac{\gamma_{out}\gamma_{in}}{\gamma_{out}+\gamma_{in}} \right) \right\} \tag{3.17}$$

It is important to conclude in equation 3.17 that to obtain f_c^{max}, the absolute values of the force factors do not need to be known since the optimal reel out and reel in speeds only depend on the ratio F_{out}/F_{in}.

The optimal relative reeling in and out speed of each F_{out}/F_{in} ratio between 0 and 100 are shown in the next graph, as the normalized maximal cycle power factor.

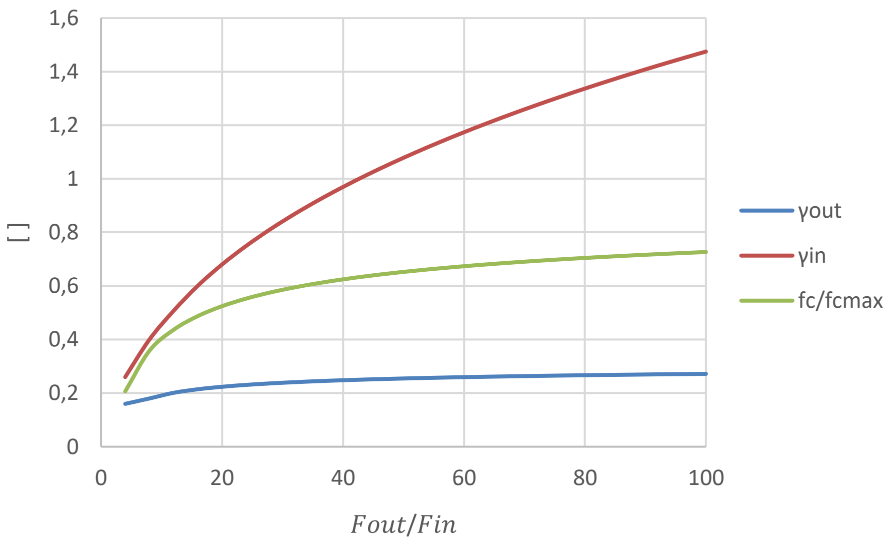

Figure 14 - Relative reel out and reel in speed and normalized cycle power factor

It is possible to observe that the relative reeling in speed is the one with the fastest growth when the F_{out}/F_{in} ratio increases. Focusing on $F_{out}/F_{in} = 100$, the optimal reel out speed is nearly 1/4 times the wind speed, a lower number than the one predicted in Loyd´s model (1/3). The optimal reel in speed is close to 1.5 times the wind speed, being 5.5 times higher than the reel out speed. In a more practical approach, the traction phase lasts nearly 5.5 times longer than the retraction phase.

The power that can be obtained for $F_{out}/F_{in} = 50$ is about 65% of the maximal power (equation 3.5) and grows to nearly 73 % when $F_{out}/F_{in} = 100$.

In conclusion, to obtain the maximal cycle power it is mandatory that the retraction phase lasts as little as possible to keep the time where no energy is produced minimal. However, the reeling in speed should be such that it does not compromise the viability of the system.

3.3. Power limitations

The mechanical power output achieved on the previous section, as well as the reel in and out speeds, are calculated without any limitations. However, the Pumping Kite system has several components that are planned for a certain given rated power such as the generator or other electronic devices. Hence, there is the need to limit the power output to ensure the correct system´s operation.

It is assumed, that for a certain wind speed v_n, the system reaches its nominal power P_{out}^n and consequently the nominal force T_{out}^n is also reached at that wind speed.

According to [31], there are two assumptions that must be taken into account:

- For wind speeds higher than v_n, both the tether force and the reel out power must be kept constant without the possibility to increase.
- Since there is a direct relation between tether force and power (equation 3.3), the reel out speed must also be kept constant.

Thus, only the reel in speed in the retraction phase can be improved.

When $v_w \leq v_n$, both γ_{out} and γ_{in} are independent of the wind and can be obtained following the equation 3.16. For the following procedures they are named as γ_{out}^n and γ_{in}^n .

At $v_w = v_n$:

$$v_{out}^n = \gamma_{out}^n v_n \tag{3.18}$$

$$T_{out}^n = \frac{1}{2}\rho v_n^2 A(1-\gamma_{out}^n)^2 F_{out} \tag{3.19}$$

$$P_{out}^n = T_{out}^n v_{out}^n \tag{3.20}$$

When the wind speed is higher than the nominal wind speed ($v_w > v_n$), the power factor is achieved following the same method as in equation 3.12 to equation 3.15:

$$E_c = (T_{out}^n - T_{in})l_c \tag{3.21}$$

$$t_c = \frac{l_c}{v_{out}^n} + \frac{l_c}{v_{in}} \tag{3.22}$$

Since $P_c = E_c/t_c$

$$\frac{P_c}{P_w A F_{out}} = f_{c,\mu} = \max_{\gamma_{in}}\left\{\left(\frac{1}{\mu^2}(1-\gamma_{out}^n)^2 - \frac{F_{in}}{F_{out}}(1+\gamma_{in})^2\right)\left(\frac{\gamma_{out}^n\gamma_{in}}{\gamma_{out}^n + \mu\,\gamma_{in}}\right)\right\} \tag{3.23}$$

Introducing a new variable, the dimensionless velocity parameter

$$\mu = \frac{v_w}{v_n} > 1 \tag{3.24}$$

The nominal values of the tether force T_{out}^n and the power P_{out}^n, both from the traction phase, are kept constant as mentioned previously. This is possible due to the adjustment that F_{out} suffers, for $\mu > 1$:

$$F_{out,\mu} = \frac{F_{out}}{\mu^2}\frac{(1-\gamma_{out}^n)^2}{\left(1-\frac{\gamma_{out}^n}{\mu}\right)^2} \tag{3.25}$$

The adjustment that F_{out} suffers can be translated by a reduction of the lift coefficient C_L.

The new γ_{out} , when the wind speed is higher than the nominal wind speed, can be obtained using the following expression:

$$\gamma_{out} = \frac{\gamma_{out}^n}{\mu}, \quad \mu > 1 \tag{3.26}$$

Figure 15 shows the dimensionless factor for the optimal reel in speed, obtained using the equation 3.23, as the optimal reel out speed, calculated following the equation 3.26. One can also find the normalized cycle power factor. All these variables in study are for $F_{out}/F_{in} = 100$.

As soon as the wind speed is above the nominal wind speed, there is the necessity to reduce the reel in speed so that the power consumed in the retraction phase do not get too large. Since the wind speed influences the reel in speed which in turn influences the power consumed, it is possible to observe that higher wind speeds translate in less power generated by the system.

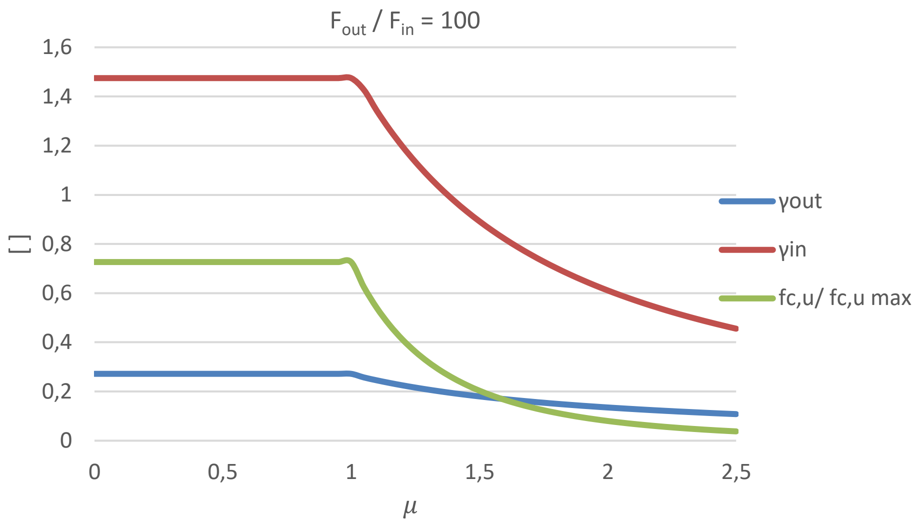

Figure 15 - Normalized cycle power factor and optimal $\gamma_{out}, \gamma_{in}$

3.4. Power Curve Construction

The power curve over one cycle of this PKG system can be obtained following two different equations: one for the wind speed being lower than or equal to the nominal wind speed and the other when the wind speed is higher than the nominal wind speed.

The nominal wind speed is set to 10 m/s, which will be used in all power curves for different F_{out}/F_{in} ratios.

For $0 < v_w < v_n$:

$$\frac{P_c}{AF_{out}} = P_w \max_{\gamma_{out},\gamma_{in}} \left\{ \left((1-\gamma_{out})^2 - \frac{F_{in}}{F_{out}} (1+\gamma_{in})^2 \right) \left(\frac{\gamma_{out}\gamma_{in}}{\gamma_{out}+\gamma_{in}} \right) \right\} \tag{3.27}$$

For $v_w > v_n$:

$$\frac{P_c}{AF_{out}} = P_w \max_{\gamma_{in}} \left\{ \left(\frac{1}{\mu^2} (1-\gamma_{out}^n)^2 - \frac{F_{in}}{F_{out}} (1+\gamma_{in})^2 \right) \left(\frac{\gamma_{out}^n \gamma_{in}}{\gamma_{out}^n + \mu\,\gamma_{in}} \right) \right\} \tag{3.28}$$

The following figure shows the power curve for $F_{out}/F_{in} = 100$. It is possible to observe that the cycle power starts to decrease for wind speeds higher than the nominal wind speed (10 m/s). This decline is perceptible since the traction power must be kept constant and the retraction power from the retraction phase increases with the increasing wind speed.

This approach to build a power curve over one cycle of a pumping kite system benefits the wind speeds close to the nominal one since it is in that range that the most power is obtained.

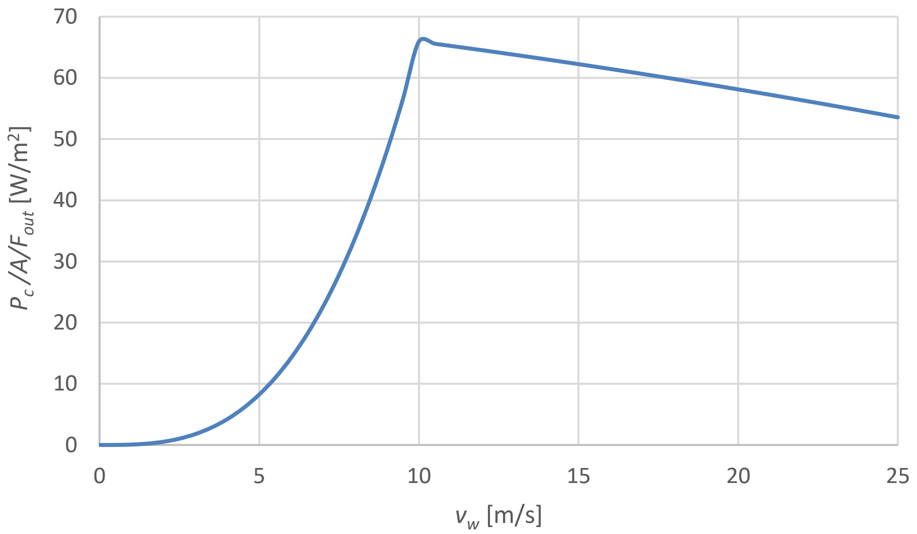

Figure 16 - Power curve of a pumping kite system over one cycle with F_{out}/F_{in}=100

Since the influence of the F_{out}/F_{in} ratios are quite notorious in the extracted power of these systems, the next figures show the power curves over one cycle for F_{out}/F_{in} equal to 20, 50 and 70 respectively.

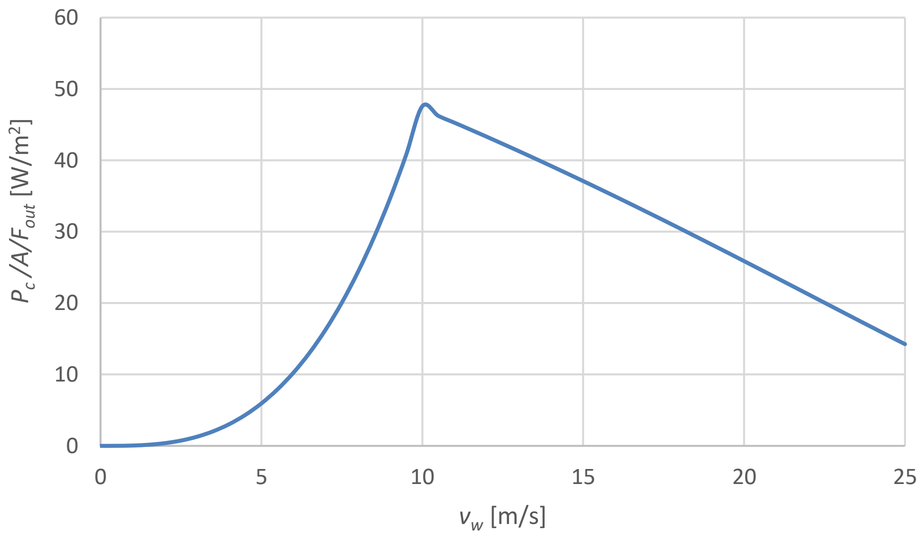

Figure 17 - Power curve of a pumping kite system over one cycle with F_{out}/F_{in}=20

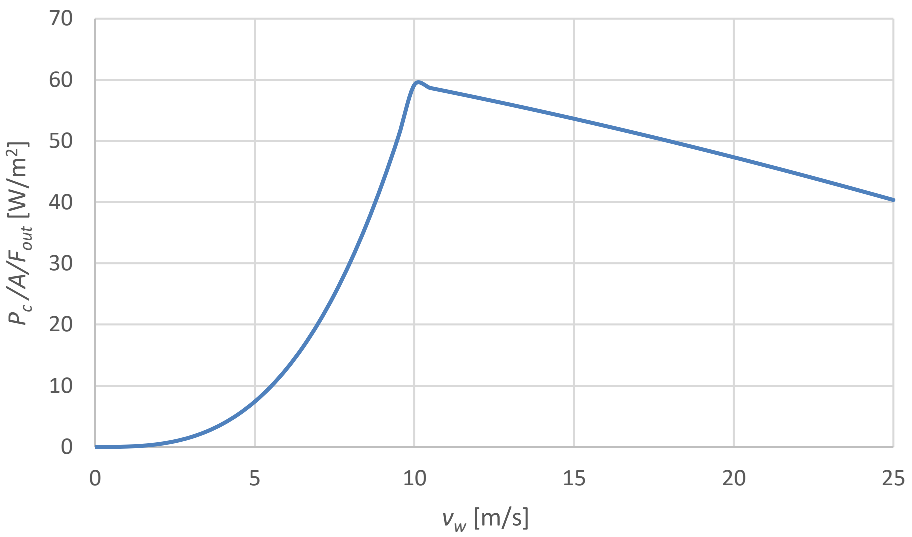

Figure 18 – Power curve of a pumping kite system over one cycle with F_{out}/F_{in}=50

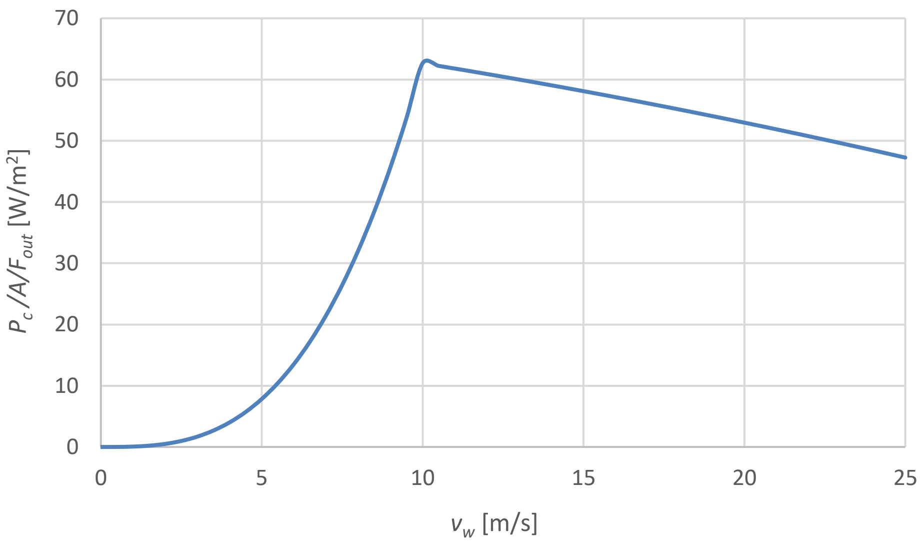

Figure 19 - Power curve of a pumping kite system over one cycle with F_{out}/F_{in}=70

Theoretically, the higher F_{out}/F_{in} ratio, the higher the power extracted during a cycle. However, ratios that are too high are physically impossible to obtain but some generals conclusions can be drawn. Ideally, one should have a $F_{out}/F_{in} = \infty$, meaning that the traction phase is so much greater that one considers the retraction phase null (time where no energy is produced). Since this is impossible to achieve, one should consider the viability of the system when projecting the F_{out}/F_{in} ratio.

The following figure compares some F_{out}/F_{in} ratios.

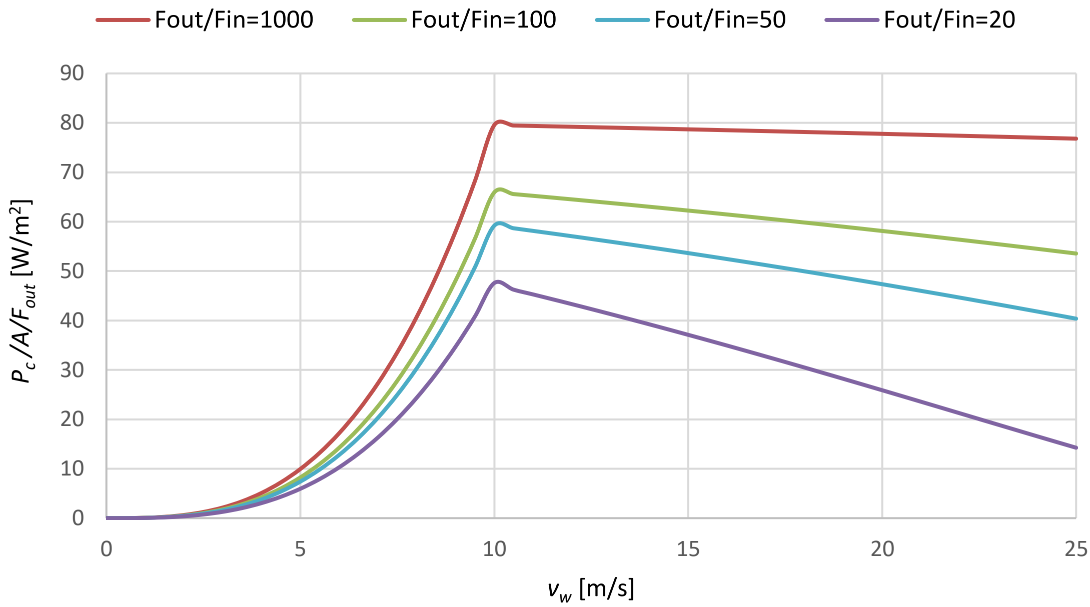

Figure 20 - Comparison of various power curves for different F_{out}/F_{in} ratios

3.5. Adjustable reel in speeds for $v_w > v_n$

In the previous section, according to equation 3.28, it becomes understandable the need to calculate different dimensionless factors γ_{in} for each wind speed above the nominal one (10 m/s), which will translate in adaptable reel in speeds for the retraction phase. One developed a method to achieve the reel in parameters.

Since certain F_{out}/F_{in} ratios are impossible to achieve, it was selected a feasible range of values to study the behavior of γ_{in}. These values of F_{out}/F_{in} are 100, 85, 70, and 50.

The power equations of γ_{in} for the different ratios are represented in the following table as well as the evolution of γ_{in} in Figure 21.

Table 1 - Power equations of γ_{in} for several F_{out}/F_{in} ratios

F_{out}/F_{in}	γ_{in} equation
50	$\gamma_{in} = 32.272 v_w^{-1,458}$
70	$\gamma_{in} = 31.264 v_w^{-1,381}$
85	$\gamma_{in} = 31.328 v_w^{-1,346}$
100	$\gamma_{in} = 31.636 v_w^{-1,321}$

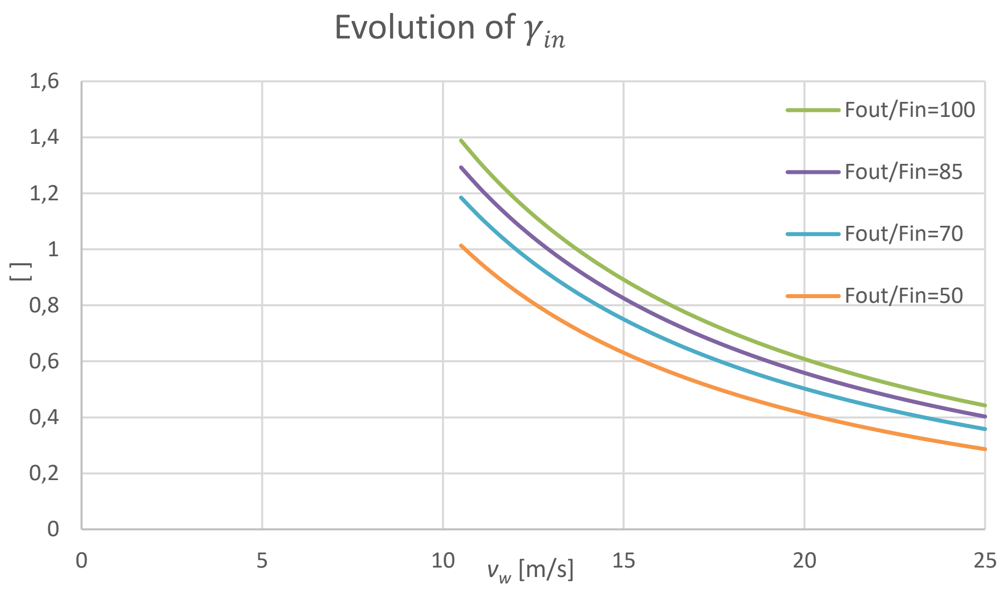

Figure 21 - Evolution of γ_{in} for different F_{out}/F_{in} ratios

With the γ_{in} equations extracted, it was possible to obtain a function including the power factors and the constants that were derived as indicate by equation (3.29).

$$\gamma_{in} = 31.6\, v_w^{0{,}1993 \ln\left(\frac{F_{out}}{F_{in}} - 2{,}2339\right)} \tag{3.29}$$

A logarithmic expression proved to be the most appropriate function for the power with the values presented above in Table 1.

This proves to be valuable for this range of F_{out}/F_{in} ratios since the flexible reel in speeds in the retraction phase for $v_w > v_n$ could only be achieved applying optimal solutions tools.

Chapter 4

Annual Power Output for Real Wind Data

This chapter studies the potential power that a pumping kite generator system can produce in a year when applied to real wind data. In Section 4.1 the wind data under analysis is described. In Section 4.2, it is presented a method to extrapolate wind speeds for different heights. Section 4.3 is where the system under test is characterized and the annual average power is calculated. In Section 4.4, the annual average power is also calculated but with a Weibull Distribution. Finally, in Section 4.5, the theoretical operating limitations of the kite´s system are presented, and statistical analyses are made.

4.1. Wind Data Characteristics

The wind data under analysis was provided by the Portuguese renewable energy company MEGAJOULE [32]. The data was collected by four anemometers installed in Portugal, but their exact location remains unknown due to terms of confidentiality. These four wind measure devices were installed in four different altitudes: 30, 50, 70 and 88 meters.

The data was collected between from 01/01/2016 to 21/12/2016 being each set of parameters collected every 10 minutes. Some parameters measured were the wind direction and the average wind speed. However, the wind´s direction was not considered in the analyses, translating into an ideal kite path and an optimistic estimation of power output due to the consideration that the wind is in the optimal direction.

Still, the objective is not to know the wind speed at the heights provided by the anemometers but at a certain maximum altitude that the kite will reach during the trajectory. For this reason, it is imperative to know the wind speed during the kite´s flight since the kite is at different elevations corresponding to different acting forces in the system.

4.2. Wind Shear Coefficient

There is a need to estimate the values of wind speed for different altitudes in order to calculate the energy produced over one cycle. This procedure can be done in several different ways. However, the most common and practical ones are the log law (equation 4.1) and the power law (equation 4.2) [33]:

$$V_{h2} = V_{h1} \frac{\ln\left(\frac{h_2}{h_0}\right)}{\ln\left(\frac{h_1}{h_0}\right)} \tag{4.1}$$

In this expression h_1 and h_2 are the reference and the target heights, respectively. V_{h1} and V_{h2} are the reference and the target height wind speeds and h_0 is the surface roughness length.

This last parameter represents the height, in meters, above ground where the wind speed is theoretically zero. One varies according to the terrain of the site in study and for that reason, many use the standard values presented in Table 2 [34].

Table 2 - Surface roughness length values for different types of terrains [34]

Terrain description	Surface roughness length, h_0 (m)
Very smooth, ice or mud	0.00001
Calm open sea	0.0002
Blown sea	0.0005
Snow surface	0.003
Lawn grass	0.008
Rough pasture	0.01
Fallow field	0.03
Crops	0.05
A few trees	0.1
Many trees, hedges, a few buildings	0.25
Forest and woodlands	0.5
Suburbs	1.5
Centers of cities with tall buildings	3.0

$$V_{h2} = V_{h1}\left(\frac{h_2}{h_1}\right)^p \tag{4.2}$$

From the previous equation representing the power law, h_1 and h_2 are the reference and the target height, respectively. V_{h1} and V_{h2} are the reference and the target height wind speeds and the new parameter p is the power law exponent. The most used value for this parameter is $p = 1/7$, considering that the terrain is flat. Nevertheless, for different types of terrains, as in the previous method, one can also use standard power law exponents.

Table 3 – Several power law exponents for different types of terrain [35]

Terrain description	Power law exponent, p
Smooth, hard ground, lake or ocean	0.10
Short grass on untilled ground	0.14
Level country with foot-high grass, occasional tree	0.16
Tall row crops, hedges, a few trees	0.20
Many trees and occasional buildings	0.22-0.24
Wooded country – small towns and suburbs	0.28-0.30
Urban areas with tall buildings	0.4

It is important to mention that the use of the standard parameters from both Table 2 and Table 3 does not necessarily mean that they are accurate to the correspondent type of terrain and consequently, that the prediction of the wind speeds will be calculated with some uncertainty associated.

The power law was the one chosen to calculate the wind speed in different heights due to the fact that is more flexible than the log law [33]. Since the provided data is divided in periods of 10 minutes each, there was the necessity to calculate a different p in each period.

However, since the conditions of the terrain under study are unknown, a method had to be developed to estimate the power law exponent p for every 10-minute period. The height of 250 *m* was the one chosen to calculate the different wind speeds for different heights along the path of the kite. The parameter p is obtained minimizing the mean square error of all estimations from the four anemometers´ heights: h: [30; 50; 70; 88].

$$V_{250} = V_h\left(\frac{250}{h}\right)^p \tag{4.3}$$

4.3. Description of the kite power system and average power

In order to understand the kite´s path, Figure 22 is presented below. This model of a pumping kite generator system represents the moment when the kite reaches its maximum height. In other words, when the tether is fully stretched. It is possible to visualize that this system, with an inclination of 30°, can reach 350 meters high. Also, the starting point is about 50 meters high.

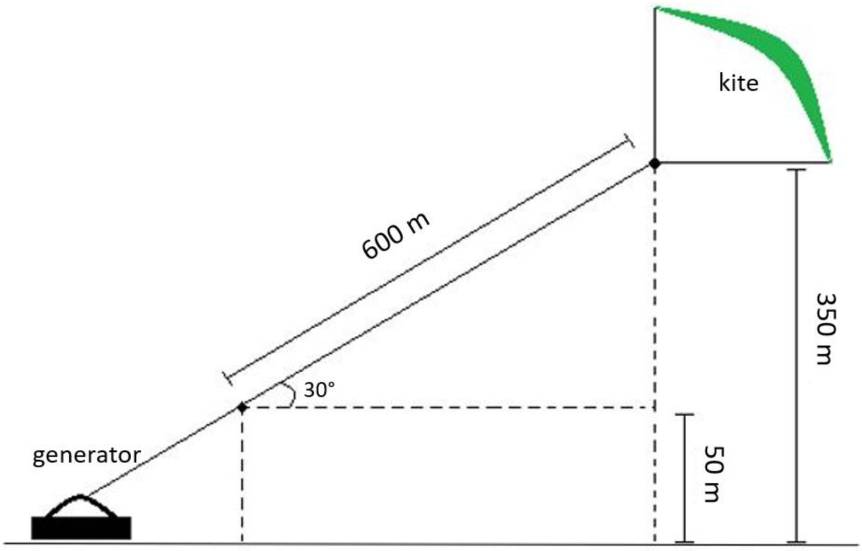

Figure 22 – Profile view of the PKG system

The PKG system under examination has a set of parameters that must be presented before any calculations, since those constraints influence the output and performance of the power cycle. Table 4 displays the selection of the ones mentioned before:

Table 4 – Parameters for the kite system under test

Parameters	Values
F_{out}	100
F_{in}	1
Density of air ρ (kg/m^3)	1.23
Area of the kite (m^2)	1
Elevation of the kite β (°)	30
γ_{out}	0.27
γ_{in}	1.475
Length of the tether (m)	700

The dimensionless force factors F_{out} and F_{in} have the value of 100 and 1, respectively. These values have the only purpose to achieve a F_{out}/F_{in} ratio of 100, example studied with detail in Chapter 3. The parameters γ_{out} and γ_{in} were calculated using equation 3.17. The value of 1.23 for the density of air ρ is the standard value at 15 ºC.

The area of the kite as well as the tether´s length can be flexible. For this study, it was selected an area of 1 m^2 and 700 meters for the length.

About the elevation of the kite there are a few considerations to provide: [36] states that in order to a kite operate with maximal value of power output, it should work in sufficiently low angles. It also states that there is a correlation between the characteristics of the terrain and the tether inclination since the power law exponent is directly related to the optimal angle of operation.

Since wind speeds increase with altitude and the tether drag increases with tether length, both factors take a significant role for determining the ideal elevation angle. The angle of 30º seems to be a good estimate, especially because the conditions of the terrain are unknown.

With all the important parameters established, the goal is to determine the power output over one cycle of the KPG system. The approach for this problem was to divide the energy obtained over one cycle in two phases: the traction phase and the retraction phase.

The first phase starts when the kite initiates his ascending movement until it reaches the highest altitude. During this period, the energy is generated when the cable is unwinding. Considering that this method is done for every second of the cycle separately, l_{c1} will be the tether´s length at the initial second and l_{c2} the length at the next second.

Based on equation 3.12:

$$E_{out} = \sum T_{out}(l_{c2} - l_{c1}) = \sum \frac{1}{2}\rho v_w^2 A((1-\gamma_{out})^2 F_{out})(l_{c2} - l_{c1}) \qquad (4.4)$$

The second phase occurs when the kite is in its highest altitude until it reaches the starting point. During this period, the power is wasted to bring the kite down. The procedure is the same as before. l_{c1} will be the tether´s length at the initial second and l_{c2} the length at the next second.

Again, based on equation 3.12:

$$E_{in} = \sum -T_{in}(l_{c2} - l_{c1}) = \sum -\frac{1}{2}\rho v_w^2 A((1+\gamma_{in})^2 F_{in})(l_{c2} - l_{c1}) \qquad (4.5)$$

The energies mentioned above are calculated every second until the end of the respective phase. At last, the power output over one cycle P is determined by dividing all the energy produced E_{out} and consumed E_{in} by the cycle time t:

$$P = \frac{E_{out} + E_{in}}{t} \tag{4.6}$$

The method used above (analyzing second by second) does not take into consideration the fact that the power output should start to drop when the wind speed surpasses the nominal wind speed (10 m/s).

Therefore, there was a necessity to understand how the power output varied for $v_w > v_n$ when compared to the maximum power obtained ($v_w = 10$).

Using the values obtained in Figure 16, the following table can be obtained:

Table 5 - Percentage variation of power output for wind speeds higher than 10 m/s

Wind Speed v_w (m/s)	P_c / AF_{out}	Percentage of maximum power output (P_{mo})
10	66.242	100.00%
11	64.974	98.09%
12	64.301	97.07%
13	63.612	96.03%
14	62.905	94.96%
15	62.181	93.87%
16	61.441	92.75%
17	60.683	91.61%
18	59.908	90.44%
19	59.117	89.24%
20	58.308	88.02%
21	57.482	86.78%
22	56.640	85.50%
23	55.781	84.21%
24	54.905	82.89%
25	54.013	81.54%

For values above 10 m/s for the wind speed, it is possible to find a function that represents the relationship between P_{mo} and the wind speed v_w, which is given by Equation 4.6:

$$P_{mo} = 1.139e^{-0.013v_w} \tag{4.7}$$

The power output of the system characterized above, over a year, can be calculated using the wind data provided by MEGAJOULE. For every 10 minutes there is a different wind speed at 250 meters of altitude and a different wind shear coefficient p. These two variables will be the only ones changing in the estimate of the power output for every iteration until the last 10 minutes of the year. Again, one must consider that when the wind speed is above the nominal one, the power obtained must be multiplied by the correspondent percentage using equation 4.6.

For the example given in this chapter, the power output of the system is the average of all the power outputs calculated every 10 minutes. One obtains the value of 2429 W with a capacity factor of 36.6%, since the maximal power output that can be extracted is 6624 W.

4.4. Statistical characterization of wind speed

The wind data provide accurate information on the characteristics of the wind in question during a year. However, it is not always possible to have this type of information and there is a need to predict the behavior of the wind. Therefore, in this section, the power output is calculated following the same procedure as before, but the wind data used is the result of a certain distribution.

The data under study can be described through a probability density function and the power output can be calculated according to the frequency of certain wind speeds. The Weibull Distribution is considered the most appropriate function to represent wind speed variations.

The following equation describes the distribution function:

$$f(v) = \frac{k}{\lambda}\left(\frac{v}{\lambda}\right)^{k-1} e^{-\left(\frac{v}{\lambda}\right)^{k}} \quad (4.8)$$

In this expression k is a shape parameter and λ is a scale parameter expressed in m/s.

Taking into account the frequency of the wind speeds and minimizing the mean squared error between the real frequency of the wind data and the Weibull distribution, it was possible to calculate $k = 1.3$ and $\lambda = 8.08$. The following figure represents Weibull distribution according to the data provided.

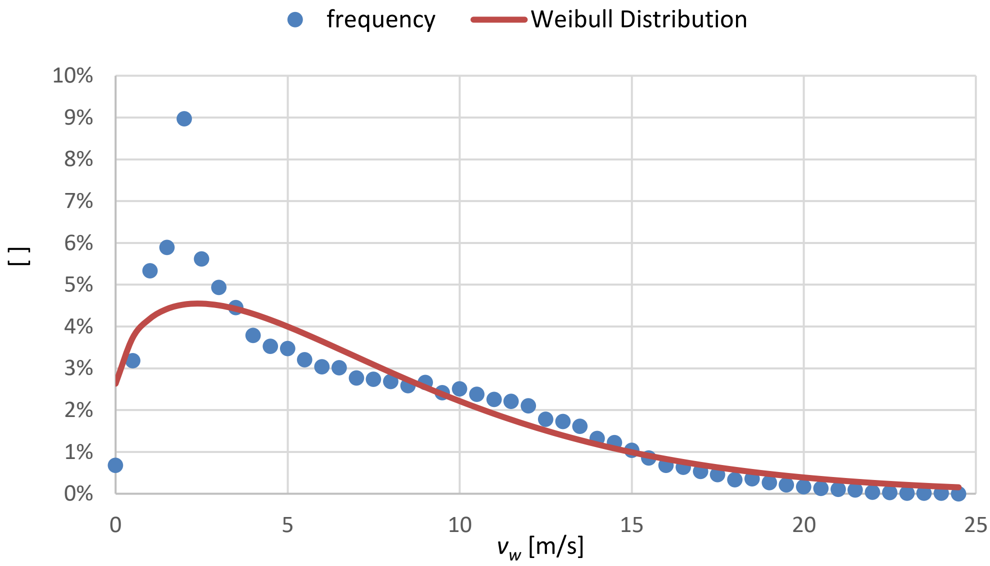

Figure 23 - Frequency of events at a certain speed and respective Weibull Distribution

To obtain the power output over the year, the power assigned to a certain wind speed based on the power curve of Chapter 3, was multiplicated by the frequency of the Weibull Distribution curve.

One obtains the value of 2523 W with a capacity factor of 38.1% for the same maximum power output.

4.5. Operating limitations

The values of power output obtained in the previous section do not take into account any kind of limitation. However, if the wind speed is too low, the correct operation of the kite is compromised since the kite cannot produce more energy in the traction phase than the energy wasted in the retraction phase. In other words, the power generated will not be rewarding.

Therefore, there is a need to define that below a certain wind speed, the kite will not be put into operation. This wind speed was defined as 5 m/s at 250 meters of altitude since this is the height that estimates all the wind speeds during the cycle power by the power law used in equation 4.3.

To understand the influence that this limitation has in the power output obtained, one presents the following figures where the power output can be visualized over the period of January 19 to January 22:

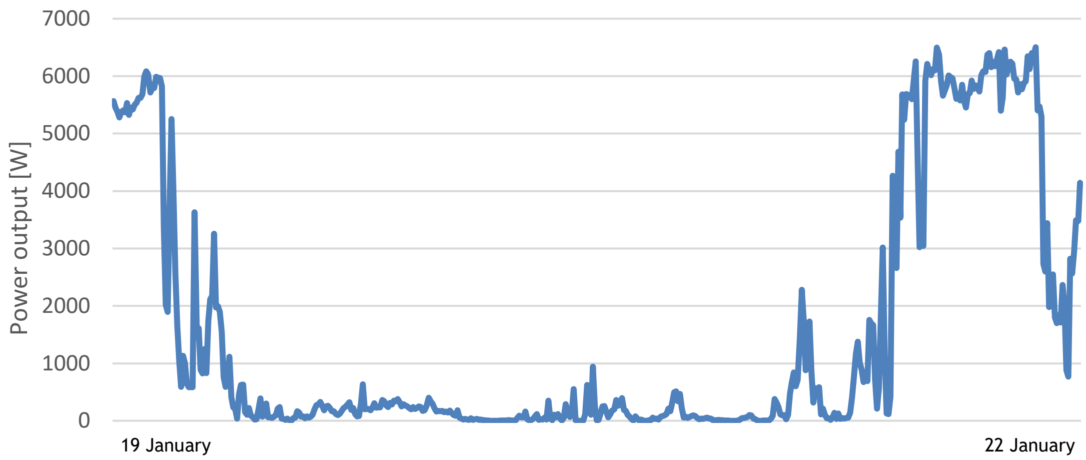

Figure 24 - Power output variation without any restrictions

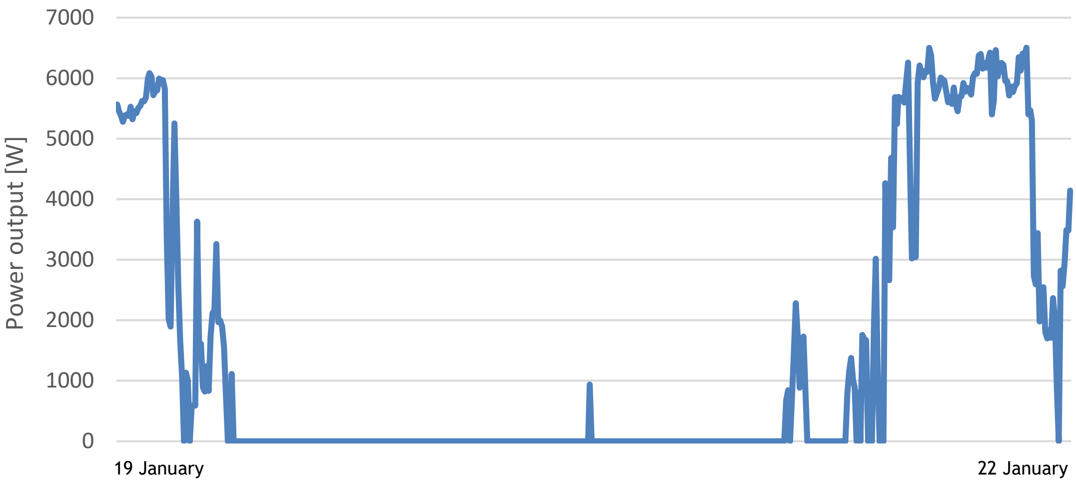

Figure 25 - Power output variation of the system when only works for $v_w > 5\ m/s$

It is possible to observe that, between the period mentioned previously, almost no energy is produced when the system works under certain limitations. Although the continuous operation would be ideal, one can also observe that the power extracted in those periods where the wind speed is too low, is minimal. Thus, will not take a major influence in the final annual average power output, as it can be seen later on.

For a correct understanding about the behavior of the wind speed in the wind data provided, Figure 26 shows the monthly average wind speed during the year and monthly average power output for each month.

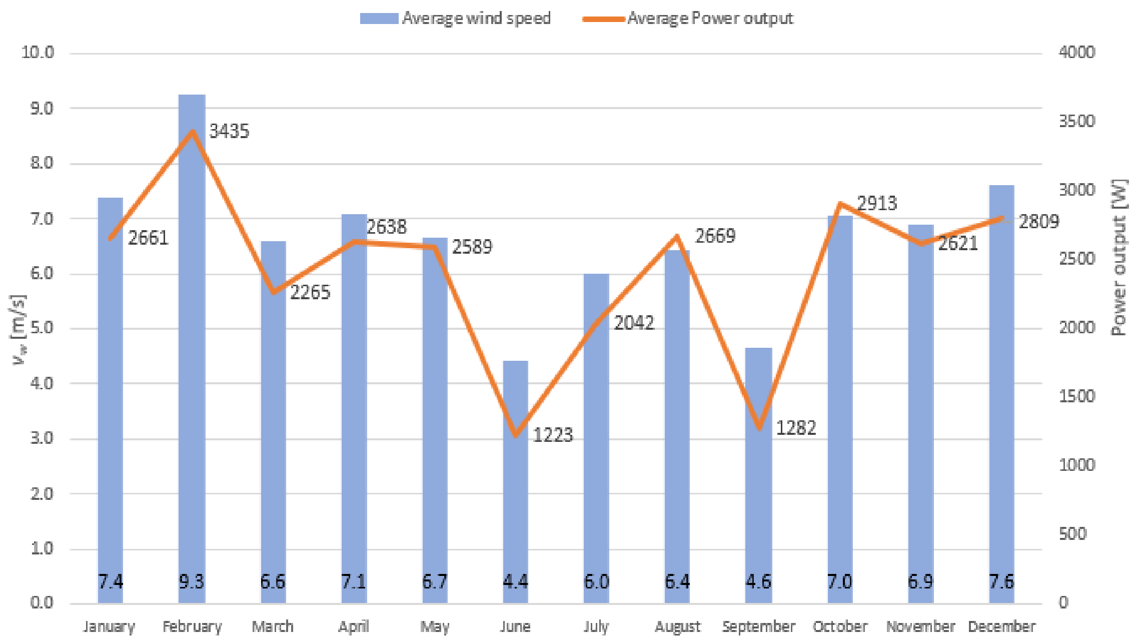

Figure 26 - Average monthly wind speed and power output during the year 2016

It is easily observed that February has the highest monthly average wind speed (9.3 m/s) in contrast with June, which has the lowest (4.4 m/s). This is directly related to the variation of the power output obtained in every month, since the higher average wind speed, the greater the power extracted.

Taking a closer examination in the month of February (Figure 27), the most productive one in terms of energy obtained, it is possible to see that almost 50% of the days averaged a wind speed equal or greater than 10 m/s. This is an ideal situation for the energy efficiency of the system as it works close to its maximum capacity.

As one could see in Chapter 3, the increase in wind speeds do not necessarily translates into greater energy outputs, since the traction power is kept constant while the retraction power further increases. One may take the example of day 5 and day 29 of February, when wind speeds are greater than 16 m/s but do not present a significantly higher power.

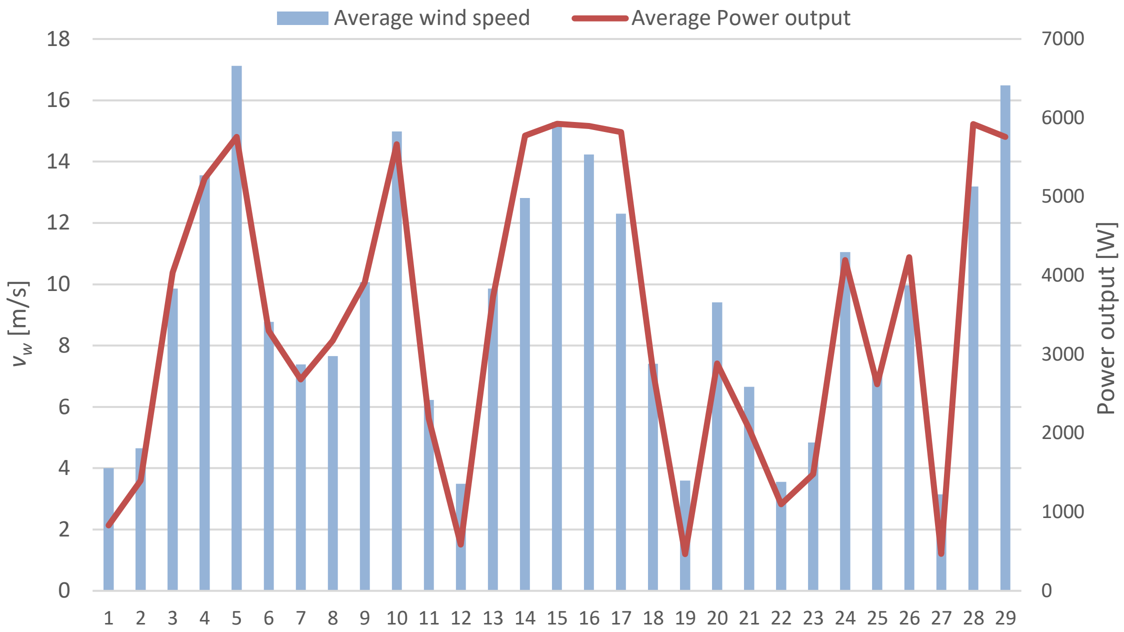

Figure 27 - Average daily wind speed and power output during the month of February

Assuming the kite does not work for wind speeds below 5 m/s, there is the necessity to calculate the power output for this new restriction. The procedure was to ignore all the power production in the periods where $v_w < 5\ m/s$.

The new values are presented in the following table:

Table 6 - Values of the Average Power Output and the respective capacity factor

	Average Power Output (W)	Capacity factor (%)
Weibull	2523	38.1%
Weibull ($v_w > 5\ m/s$)	2434	36.7%
Real Wind Data	2429	36.6%
Real Wind Data ($v_w > 5\ m/s$)	2321	35%

One can conclude that the estimations of the power output with the provided real wind data and with the Weibull Distribution are quite similar. Also, when wind speeds below 5 m/s are not considered, the average power output falls slightly but not in a significant way. This fact proves that velocities below 5 m/s do not contribute significantly for the optimization of the system since the power extracted in those wind speeds are very low.

Regarding the question of possible launching and landing approaches for various wind systems, one must evaluate how many times the kite worked for a certain period of time, in order to comprehend the feasibility of the operation.

[37] shows three different approaches about this matter: Vertical take-off (VTOL), catapult and rotating arm, all represented in the following figure:

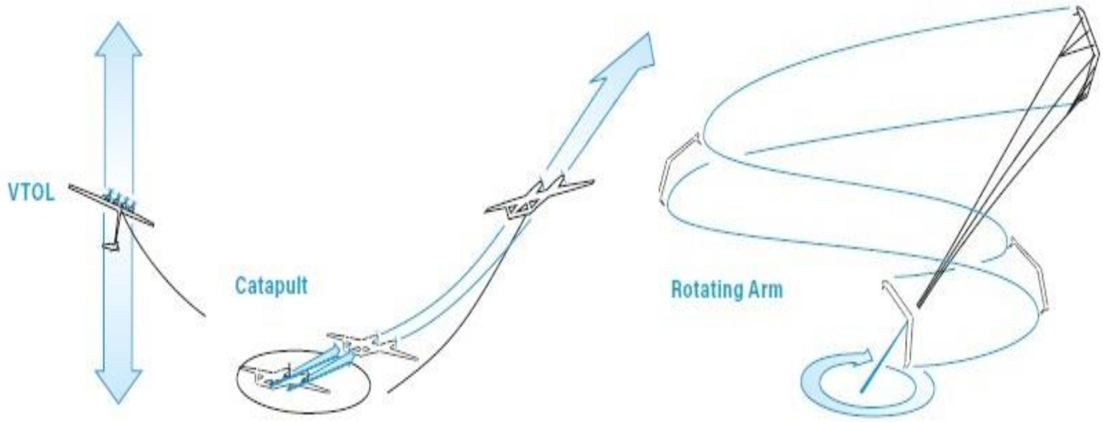

Figure 28 -Launching and landing approaches: Vertical take-off on the left, Catapult in the center, Rotating arm on the right [37]

The Vertical take-off is used mainly for airborne wind systems but can also be used in on-ground ones. This concept uses thrust from additional rotors to lift and maneuver the wing during take-off and landing.

For the catapult launch, the method can be used either in on-ground or airborne wind systems. It consists in projecting the power device in an ascending way in order to achieve a certain altitude to start the cycle.

The rotating arm approach is only used for on-ground systems in which the power device is launched into the air using a helical movement.

Since the approaches mentioned before are resource intensive, it was necessary to make a statistical analyze regarding the continuous working time of the system. Recalling that the kite´s system only works with wind speeds greater than 5 m/s, the number of times it was operating uninterruptedly was recorded. Considering that 1440 minutes is equivalent to one day, the values presented on Table 7 were obtained from the real wind data set.

Table 7 - Number of occurrences in consecutive operating time intervals

Consecutive Operating time interval (min)	Number of occurrences
[0,1440]	1687
[1440,2880]	27
[2880,4320]	13
[4320,5760]	2
[5760,7200]	2

As one may observe in the previous table, the number of times that the machine worked consecutively between 0 and 1440 minutes (1 day) is far superior to the other number of occurrences. In fact, of the 1687 times that the kite worked consecutively in the time interval of one day, 75% occurred during the first hour. For that reason, a closer examination was made to understand the on-and-off stages of the system during an hour:

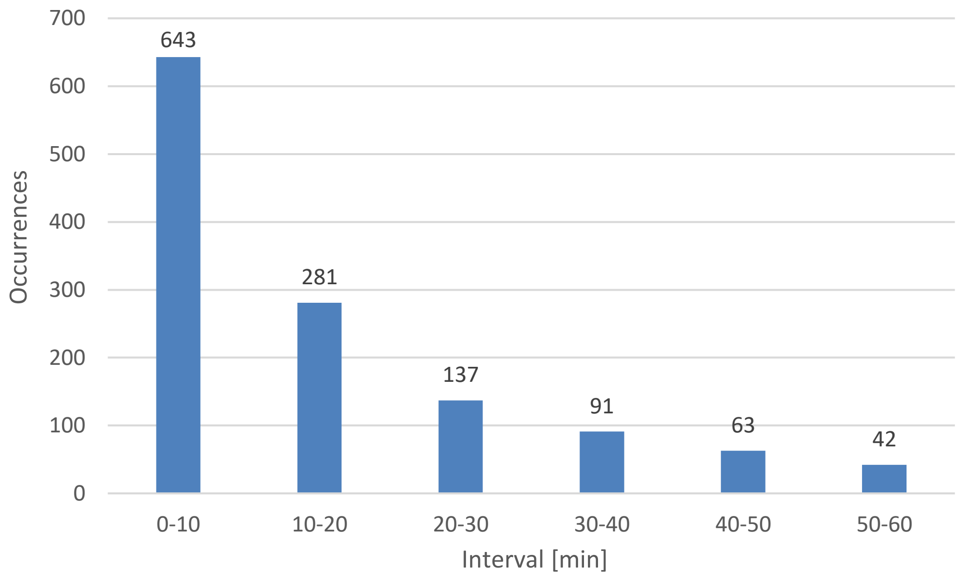

Figure 29 - Number of on-and-off stages for every 10 minutes during an hour

From this figure, it can be concluded that 50% of the occurrences happened in the first 10 minutes where the system switched immediately to an off-stage. It is also visible that obtain consecutively greater working periods of time becomes more difficult, since it was very rare to have large periods with wind speeds greater than 5 m/s at 250 meters height.

These facts raise an importance to know if the pumping kite generator systems should operate during short periods of time, considering the cost-benefits of the launching and landing approaches.

Chapter 5

Conclusions and Future Work

Airborne wind energy is currently a very promising area regarding sustainable production of electrical energy. All the investment in researches by several companies and universities contributed to achieve breakthroughs and developments, especially on aerodynamics and control technologies. However, since the output energy is at a preliminary stage, due to the majority of the companies developing AWES only have prototypes and are in experimental phases, an estimation of the energy production is presented.

Firstly, background research was an important step to get a better understanding of the current paradigm in the AWES industry. Several corporations and small companies are presented, and their works characterized. The technologies and devices already tested are classified according to the location where the power is generated and the aircrafts that are used. Although the plane-type of kite is easier to control and adjust its course, there are numerous advances considering the kite´s automatic movement. Also, some systems mentioned in this thesis are being developed to reach megawatt values in terms of nominal power.

It was also presented a more detailed overview regarding the pumping kite generator system, with a fixed ground station. With a controlled tethered wing, the system reaches heights where the wind speed is greater and takes advantage of this to produce more energy. The acting forces on the system were derived in order to obtain the mechanical power. The traction and retraction phase of the pumping cycle were studied. The theory approached showed that mechanical efficiency is determined by the two force factors F_{out} and F_{in}. A power curve of the system was obtained taking into account the wind speeds to which the system has been subjected. Several F_{out}/F_{in} ratios are tested to understand the changes in the respective power curves and the reeling in and out speeds are optimized, due to the fact that these speeds take a major role in the power produced in the traction phase and the power wasted in the retraction one.

Operating limitations were also defined due to the fact that this type of systems cannot operate in every condition. It was established that the kite did not work under wind speeds below 5 m/s.

A method where the produced energy is calculated separately is developed and put into practice using real wind data. The annual average power output is calculated using two different wind analyses: applying the method developed directly into the wind data and using a Weibull Distribution to describe the behavior of the wind. A comparison of the power output was also made if the kite worked in all conditions and if only worked for wind speeds above 5 m/s. The restriction presented proved that the energy produced with limitations did not significantly changed compared to the one without any restrictions.

The average power output when the methodology developed was applied to a Weibull Distribution was 2523 W with a capacity factor of 38.1%, and 2429 W with a capacity factor of 36.6% when applied to real wind data for every 10 minutes, regarding the wind speed. When the limitations were imposed (system not working with wind speeds below 5 m/s), the power obtained was 2434 W with a capacity factor of 36.7% for the Weibull Distribution, and 2321 W with a capacity factor of 35% for real wind data.

All the estimations of the annual power output followed an optimistic prediction since the wind speed direction was not taken into account. Also, it was considered that for every 10 minutes that the kite flew, the cycles were never interrupted.

A statistical analysis of the wind was done in order to visualize the months where the produced energy was greater. January, October and December were the ones with the largest power outputs. Also, the number of times that the kite worked consecutively during certain periods was presented, since the launching and landing approaches require significant resources. It was possible to visualize that the of on-and-off stages that the system suffered during the year, nearly 75% happened when the kite worked only for one consecutive hour. Considering this first hour of continuous operation, 50% of the occurrences where the system turned off happened in the first 10 minutes.

The airborne wind systems still integrate a vast number of variables which can be optimized in order to reach higher maximal power outputs. This makes the design and study of the system an intricate project, constantly changing.

For future development, favorable F_{out}/F_{in} ratios to maximize the energy obtained may be difficult to obtain and tests can be made to achieve the best ones. The optimal tether length and elevation angle can be calculated depending on those ratios. Autonomous adjustable reel in and out speeds can be projected in order to change with wind variations.

At last, with all the parameters defined, an estimation of the system´s cost can be predicted in order to calculate the levelized cost of energy and compare with another renewable energies.

References

[1] Pieprzyk, B., N. Kortlüke, and P.R. Hilje, *The impact of fossil fuels. Greenhouse gas emissions, environmental consequences and socio-economic effects*. 2009.

[2] World Wind Energy Association WWEA, 2018.

[3] Clímaco, F. *História da energia eólica e suas utilizações*. 2009; Available from: https://pedesenvolvimento.com/2009/07/15/historia-da-energia-eolica-e-suas-utilizacoes/.

[4] Magedi Moh. M. Saad, N.A., *Comparison of Horizontal Axis Wind Turbines and Vertical Axis Wind Turbines*. 2014.

[5] Ahmad M., M.A., M. and Tharwat, *Vertical axis wind turbine modeling a*. 2006.

[6] Paiva, F.A.F.a.L.T., *UPWIND*. 2017.

[7] Mann, S., *An Introduction to Airborne Wind Technology and Cost Reduction Trends*. 2019.

[8] 2015; Available from: https://phys.org/news/2015-02-turbines-electricity.html.

[9] Energies, A.

[10] Diehl, M., *Airborne wind energy: Basic concepts and physical foundations*, in *Airborne wind energy*. 2013, Springer. p. 3-22.

[11] Cherubini, A., *Advances in Airborne Wind Energy and Wind Drones*. PhD, Scuola Superiore Sant'Anna, Pisa, Italy, 2017.

[12] Loyd, M.L., *Crosswind kite power (for large-scale wind power production)*. Journal of energy, 1980. **4**(3): p. 106-111.

[13] De Lellis, M., R. Saraiva, and A. Trofino. *Turning angle control of power kites for wind energy*. in *52nd IEEE Conference on Decision and Control*. 2013. IEEE.

[14] Sugimoto, T. *Mechanics of classical kite buggying or how mr. pocock gained* 9m/s *by his charvolant*. in *The Seventh Asia-Pacific Conference on Wind Engineering*. 2009.

[15] Cherubini, A. and M. Fontana, *Assessment of Megawatt-Scale Wind Energy Drone Generators at Jet Stream Altitude*. 2017, Review.

[16] Rautakorpi, P., I. Argatov, and R. Silvennoinen, *Estimation of the mechanical power of a kite wind generator*. Renewable Energy for Sustainable Future. iConcept Press Ltd., USA, 2013.

[17] Fagiano, L. and M. Milanese. *Airborne wind energy: an overview*. in *2012 American Control Conference (ACC)*. 2012. IEEE.

[18] Schmehl, R., *Airborne wind energy: advances in technology development and research*. 2018: Springer.

[19] Power, A., *Airborne wind energy*. 2015, Springer.

[20] EnerKite.

[21] Bormann, A., et al., *Development of a three-line ground-actuated airborne wind energy converter*, in *Airborne wind energy*. 2013, Springer. p. 427-436.

[22] KitePower. Available from: http://www.kitepower.eu/.

[23] *TU Delft*. Available from: https://www.tudelft.nl/.

[24] Shell. Available from: https://www.shell.com/inside-energy/kite-power.html.

[25] *e-Kite*. Available from: http://www.e-kite.com.

[26] Canale, M., L. Fagiano, and M. Milanese, *KiteGen: A revolution in wind energy generation*. Energy, 2009. **34**(3): p. 355-361.

[27] *Wired: generating power from kites*. Available from: www.wired.com.

[28] *KiteGen Research*.

[29] *Makani Power*.

[30] *Omnidea*.

[31] Luchsinger, R.H., *Pumping cycle kite power*, in *Airborne wind energy*. 2013, Springer. p. 47-64.

[32] *MEGAJOULE*. Available from: http://www.megajoule.pt/?lingua=pt.

[33] Ray, M., A. Rogers, and J. McGowan, *Analysis of wind shear models and trends in different terrains*. University of Massachusetts, Department of Mechanical and Industrial Engineering, Renewable Energy Research Laboratory, 2006.

[34] Manwell, J.F., J.G. McGowan, and A.L. Rogers, *Wind energy explained: theory, design and application*. 2010: John Wiley & Sons.

[35] Bechrakis, D. and P. Sparis, *Simulation of the wind speed at different heights using artificial neural networks*. Wind Engineering, 2000. **24**(2): p. 127-136.

[36] Argatov, I. and R. Silvennoinen, *Structural optimization of the pumping kite wind generator*. Structural and Multidisciplinary Optimization, 2009. **40**(1): p. 585.

[37] Burkhard Rieck, M.R., Ashwin Candade, Alexander Bormann, *Comparison of Launching and Landing Approaches*, in *Airborne Wind Energy Conference*. 2017.